Journal of Solid State Chemistry 184 (2011) 1608–1613

Contents lists available at ScienceDirect

Journal of Solid State Chemistry

journal homepage: www.elsevier.com/locate/jssc

Neutron diffraction study and superparamagnetic behavior of $ZnFe_2O_4$ nanoparticles obtained with different conditions

V. Blanco-Gutierrez [a], E. Climent-Pascual [a], M.J. Torralvo-Fernandez [a], R. Saez-Puche [a,*], M.T. Fernandez-Diaz [b]

[a] Departamento Química Inorganica, Facultad de Ciencias Químicas, Universidad Complutense de Madrid, Ciudad Universitaria, 28040 Madrid, Spain
[b] Institut Laue-Langevin, B.P. 156, F-38042 Grenoble Cedex 9, France

ARTICLE INFO

Article history:
Received 7 January 2011
Received in revised form
11 April 2011
Accepted 17 April 2011
Available online 28 April 2011

Keywords:
Zn-ferrite
Nanoparticles
Neutron diffraction
Inversion degree
Superparamagnetism

ABSTRACT

Spinel-type (S.G.= $Fd\bar{3}m$) $ZnFe_2O_4$ fine particles with sizes from 4 to 19 nm prepared by solvothermal and microwave-assisted solvothermal methods have been studied by neutron powder diffraction at room temperature. The cation distribution corresponding to mixed spinel structure $(Zn^{2+}_{1-x}Fe^{3+}_x)[Fe^{3+}_{2-x}Zn^{2+}_x]O_4$ along with the unit cell parameter has been estimated after Rietveld refinement of the obtained neutron diffraction data for all the samples. It has been found that the inversion degree parameter (x) takes values between 0.11 and 0.20 depending not only on the particle size but also on the synthesis conditions as well. All the samples behave as superparamagnetic with an effective magnetic moment per particle (μ_{SP}) from 7.0×10^2 to 7.7×10^3 μ_B. The sample obtained by microwave assistance displays a different magnetic behavior as the ZFC and FC magnetic susceptibility and the magnetization versus applied field hysteresis loop measured at 5 K suggest. This is related with the dipole interactions that are a consequence of the higher inversion degree and μ_{SP}.

1. Introduction

Nanotechnology can be considered as one of the most fruitful current scientific fields due to the new physical and chemical properties discovered in nanomaterials, which are consequences of the finite size effects [1–3]. An example can be found in single-domain magnetic nanoparticles that display superparamagnetism above a certain temperature (named as blocking temperature, T_B), characterized by the absence of coercive field (H_C) and S-shaped magnetization (M) versus applied field (H) curves [4,5]. This interesting feature makes them to be under study to explore their potential applications in several technological fields such as magnetism, electronics or biomedicine [6–10]. Some of the most studied magnetic materials correspond to ferrite compounds. In this sense, it has been observed that $ZnFe_2O_4$ compound presents an intriguing magnetic behavior when it is nanosized [11]. Zn-ferrite crystallizes with spinel structure (S.G. = $Fd\bar{3}m$, a=8.44 Å) in which the O^{2-} ions are arranged in a cubic close packing occupying 1/8 of the tetrahedral (A) and 1/2 of the octahedral (B) interstitial sites [12]. When $ZnFe_2O_4$ compound is prepared in the microscopic range, it presents antiferromagnetic behavior below T_N=10 K [13] due to a cation distribution corresponding to normal spinel $(Zn^{2+})[Fe^{3+}_2]O^{2-}_4$ (where () refers to A-sites and [] to B-sites). The Fe^{3+} ions are located in B-sites yielding two sublattices with opposite magnetic moment resulting in a zero net magnetic moment. However, when it is prepared in the nanoscale, the energy associated to the low particle size favors a mixed cation distribution in which the Zn^{2+} and Fe^{3+} ions are distributed along the A and B sites giving rise to the mixed spinel structure $(Zn^{2+}_{1-x}Fe^{3+}_x)[Fe^{3+}_{2-x}]O^{2-}_4$, where x is the inversion degree [14,15]. The two magnetic Fe^{3+} sublattices are therefore decompensated giving a non-zero net magnetic moment of the particle. This ferrimagnetic behavior is fully determined by the inversion degree that has been found to depend not only on the particle size but also on the synthesis method [16–18]. Hence, it is crucial to get information about the inversion degree in order to understand the magnetic behavior of the $ZnFe_2O_4$ compound. This parameter could be elucidated from the X-ray diffraction patterns as it is reflected in the (2 2 0)/(4 0 0) intensities ratio [19] but it seems to be difficult in the case of the Zn-ferrite as Zn^{2+} and Fe^{3+} ions present very similar structure factors. Thereby, it is necessary the employment of other techniques such as Mössbauer spectroscopy, XAFS measurements, nuclear magnetic resonance or EELS that offer accurate information about the Fe^{3+} occupancy [18,20–22] In this sense, the neutron diffraction has been found to be one of the most useful techniques, which not only reveals the cation distribution [23,24] but also indicates the unit cell parameter after Rietveld refinement of the obtained data.

* Corresponding author. Fax: +34 91 394 43 52.
E-mail address: rsp92@quim.ucm.es (R. Saez-Puche).

0022-4596/$ - see front matter © 2011 Elsevier Inc. All rights reserved.
doi:10.1016/j.jssc.2011.04.034

In this work, we present the influence of the particle size and the synthesis conditions in the inversion degree that has been calculated after Rietveld refinement of the neutron powder diffraction data, for nanoscaled $ZnFe_2O_4$ samples obtained by the solvothermal and microwave assisted solvothermal methods.

2. Experimental section

2.1. $ZnFe_2O_4$ nanoparticles obtained by solvothermal method

The synthesis of three samples with different particle sizes, Z4 (4 nm), Z11 (11 nm) and Z19 (19 nm), was carried out following the experimental details explained in a previous work [25]. Stoichiometric amounts of iron and zinc nitrates were dissolved in ethylene glycol in a concentration of 10^{-4} mol/ml in the case of Z4 sample and 10^{-5} mol/ml for Z11 and Z19 samples. Afterwards, KOH was added as the precipitant agent (2.0 M for Z4 sample and 0.5 M for Z11 and Z19 samples) until pH=11, obtaining a brown mixture that was transferred into an autoclave to be treated under different solvothermal conditions (at 160 °C for 2 h for Z4 or 24 h for Z11 and at 200 °C for 288 h for Z19). The obtained precipitates were recovered after filtering and washing with distilled water.

2.2. $ZnFe_2O_4$ nanoparticles obtained by microwave-assisted solvothermal method

In order to obtain the Z14MW sample (14 nm), stoichiometric amounts of iron and zinc nitrates were dissolved in ethylene glycol in a concentration of 10^{-5} mol/ml to add later KOH 0.5 M until pH=11. The obtained mixture was transferred into an autoclave that was placed in a microwave synthesizer (ETHOS 1, by Milestone) operating at 50 Hz and 1000 W to be treated at 200 °C (heating rate of 10 °C/min) for 3 h. Afterwards, the obtained product was filtered and washed with distilled water.

2.3. Characterization techniques

The structural phases of the samples were identified by X-ray powder diffraction employing a Siemens D-5000 diffractometer with Cu$K\alpha$ radiation. Microstructural characterization was evaluated by transmission electron microscopy (TEM) using a JEOL-2000FX microscope working at 200 kV. Neutron diffraction measurements were carried out on the high resolution powder diffractometer D2B (λ=1.594 Å) at the Institute Laue-Langevin (Grenoble, France). The powder was placed in a cylindrical vanadium can of 11 mm diameter and 40 mm height, and data were collected in the 2θ range between 6° and 160° in steps of 0.05° at room temperature and analyzed by the Rietveld method using the *FullProf* program. Diffraction peaks were fit with the Thompson–Cox–Hastings pseudo-Voigt function fixing the profile parameters V and W to the D2B instrumental resolution values, and refining the U and the cubic harmonic functions (K_{00}, K_{41}, K_{61} and K_{81}) to take account of the Lorentzian size broadening for the Laue class $m3m$. The background was determined by means of a polynomial function. The thermal parameters were described as an overall Debye–Waller factor [26]. Magnetic measurements were done in a Quantum Design XL-SQUID magnetometer in the temperature range of 4–300 K up to 5 T. Magnetic susceptibility was measured after cooling the sample at 5 K in zero-field cooling (ZFC) and in the case of field-cooling measurements (FC), the sample was cooled in the presence of a 500 Oe field down to 5 K.

3. Results and discussion

The X-ray diffraction patterns showed in Fig. 1 indicate that the four ferrite samples were obtained as single spinel phase. Moreover, a broader diffraction maxima can be seen from Z19 to Z4 revealing a decrease in particle size. In this sense, the particle size has been estimated from the Scherrer formula [27]:

$$D = \frac{0.9\lambda}{\beta\cos\theta}$$

where λ corresponds to the Cu$K\alpha$ radiation, β is the full width at half max. for a reflection maximum located at 2θ) obtaining values of 4.0, 11.0, 13.5 and 18.0 nm for Z4, Z11, Z14MW and Z19 samples, respectively.

In Fig. 2 it can be observed representative TEM images corresponding to the four samples. The estimated mean particle size values obtained after measuring 100 particles of each sample are collected in Table 2 and agree well with those determined from the X-ray diffraction patterns. The TEM images show a homogenous particle size for all of them and in the case of the sample obtained by microwave assistance, a roughed particle surface can be observed (Fig. 2c). On the other hand all the samples present a rounded polyhedral morphology.

The structures of $ZnFe_2O_4$ nanoparticles obtained under solvothermal conditions and by microwave assistance have been studied by neutron powder diffraction at room temperature (see Fig. 3). The diffraction patterns were refined using the $Fd\bar{3}m$ space group and the site occupancies were constrained between cations on the same lattice site and between A- and B-sites. The refined site occupancy and the fitting factor for each sample are shown in Table 1. The unit cell parameter and cation distribution corresponding to mixed spinel structure have been estimated after Rietveld refinement of the data (values collected in Table 2), and their evolution with the particle size is shown in Fig. 4. It can be seen an increasing inversion degree from Z19 to Z11, which is consistent with the general trend of increasing with the reduction of the particle size seen in the previous work [28]. On the other hand, taking into account the Z14MW particle size, this sample seems to present a slightly higher inversion degree (x=0.20) compared with the rest of the samples, revealing that the microwave energy supplied during the synthesis induces a more random cation

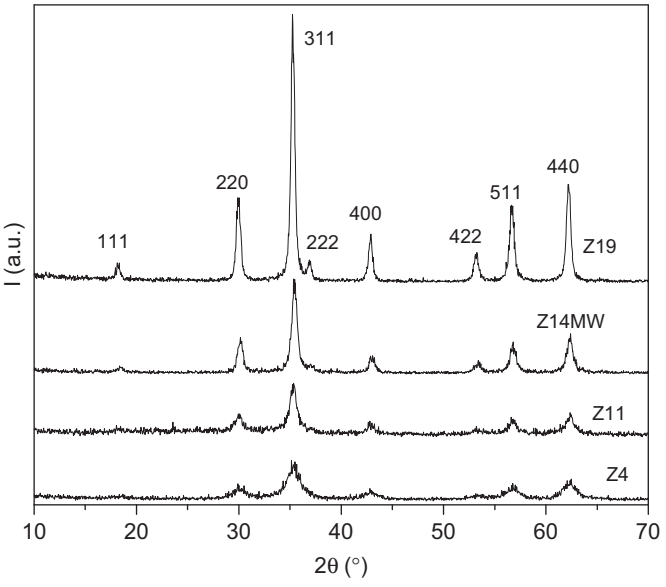

Fig. 1. X-ray diffraction patterns corresponding to $ZnFe_2O_4$ samples with particle sizes from 4 to 19 nm.

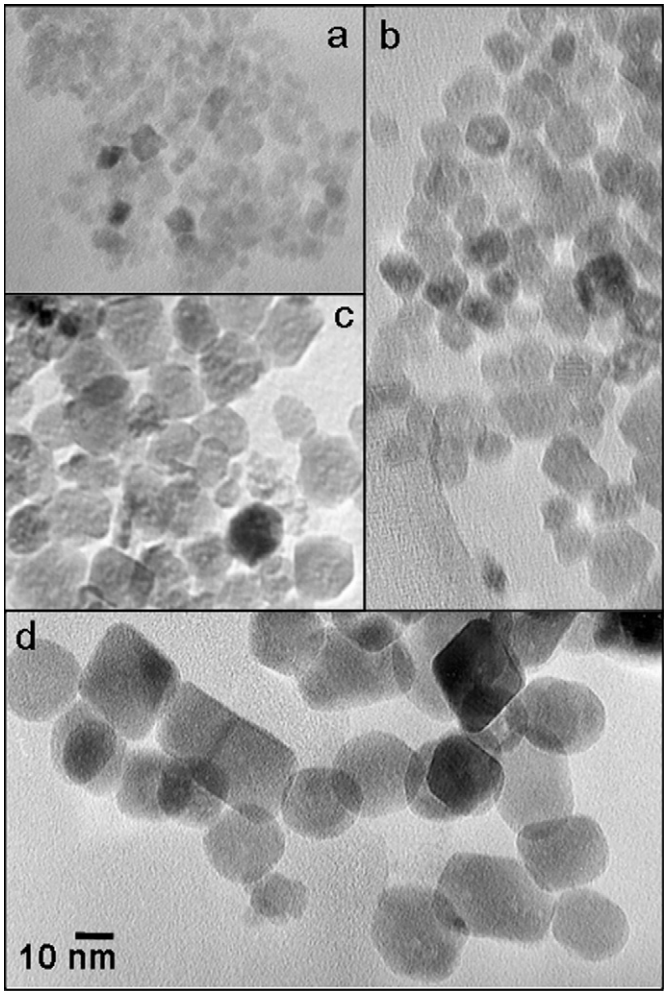

Fig. 2. Representative TEM micrographs of Z4 (a), Z11 (b), Z14MW (c) and Z19 (d) samples. All the shown images present the same scale.

distribution in the spinel structure. This corroborates the previously reported [18] influence of the synthesis conditions on the inversion degree. The Z4 sample exhibits a low inversion degree, which is probably due to the low particle size. As it has been previously reported from XPS results, the surface presents lower inversion degree than the bulk [23,29]. This has been justified under the consideration of the relatively easy structural reorganization of the surface because the cations located on it can satisfy their lack of coordination from the surrounding species of the atmosphere. In this sense, as it is well known that Zn^{2+} ions tend to present tetrahedral coordination, when the surface to volume ratio increases, there is an augment of the proportion of Zn^{2+} in tetrahedral sites leading to a reduction of the inversion degree [23,29]. This effect will be visualized in the case of very small particles, like those of Z4 sample, where the surface effect becomes more important than the bulk one.

In Fig. 4 it can be seen as well the evolution of the unit cell parameter of the samples with different particle size and inversion degree. It is well known that the large surface/volume ratio gives rise to softening of the lattice vibrations, and consequently there is an expansion of the lattice parameter [30]. This trend with the decreasing particle size can be visualized in Fig. 4. Z19 sample is the

Table 1
Refined site occupancy and fitting factor for the samples obtained by the traditional solvothermal method and the sample obtained by microwave assistance.

Atom	*Site*	*Sample*			
		Z4	Z11	Z14MW	Z19
$Zn_A(1)$	8*a*	0.840(8)	0.809(6)	0.802(6)	0.887(5)
$Fe_A(1)$	8*a*	0.160(8)	0.191(6)	0.198(6)	0.113(5)
$Fe_B(1)$	16*d*	0.5	0.5	0.5	0.5
$Fe_B(2)$	16*d*	0.420(4)	0.404(3)	0.401(3)	0.4434(24)
$Zn_B(1)$	16*d*	0.080(4)	0.096(3)	0.099(3)	0.0566(24)
O	32*e*	1	1	1	1
χ^2		1.890	1.932	1.928	2.300

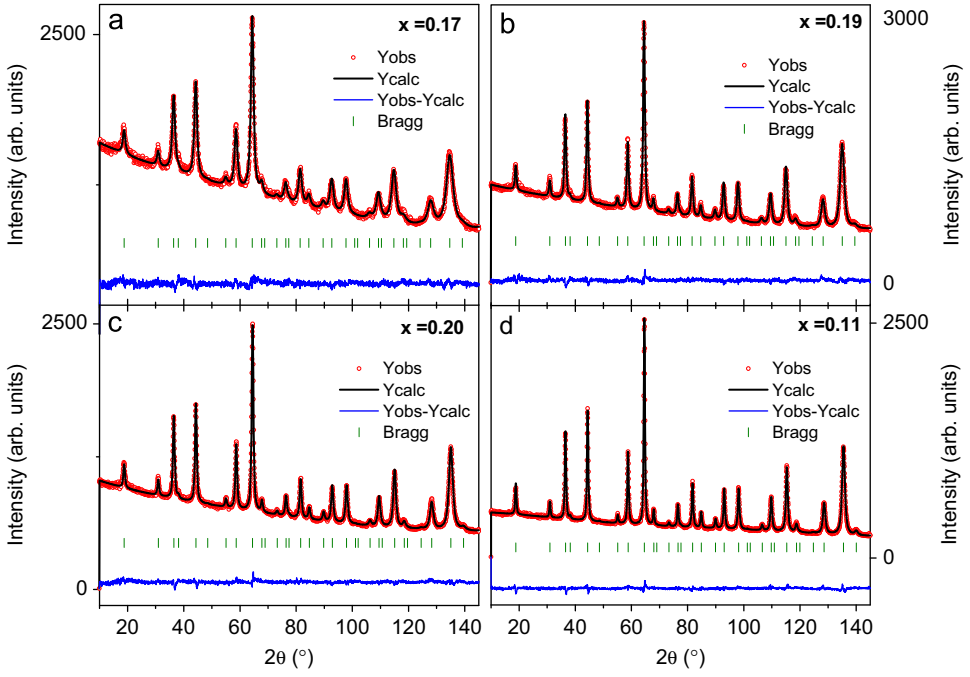

Fig. 3. Rietveld refinement of the neutron diffraction patterns obtained at room temperature for Z4 (a), Z11 (b), Z14MW (c) and Z19 (d) samples.

Table 2
Cation distribution, unit cell parameter and magnetic parameters for the samples obtained by the traditional solvothermal method and the sample obtained by microwave assistance.

Sample	D^a (nm)	Cation distribution	a^a (Å)	x^a	$T_B{}^a$(K)	$H_{C,5}{}^a$ (Oe)	$\mu_{SP}{}^a$ (μ_B)	K^a(erg/cm^3)	$M_{S,5}{}^a$(μ_B)
Z4	4.0 (1)	$(Zn_{0.83}Fe_{0.17})[Fe_{1.83}Zn_{0.17}]O_4$	8.46498 (15)	0.17	18	106	7.0×10^2	3.4×10^5	2.1
Z11	11.0 (3)	$(Zn_{0.81}Fe_{0.19})[Fe_{1.81}Zn_{0.19}]O_4$	8.45367 (10)	0.19	22	220	1.9×10^3	2.3×10^5	2.0
Z14 MW	13.5 (3)	$(Zn_{0.80}Fe_{0.20})[Fe_{1.80}Zn_{0.20}]O_4$	8.45256 (10)	0.20	35	215	7.7×10^3	1.7×10^5	2.4
Z19	19.0 (4)	$(Zn_{0.89}Fe_{0.11})[Fe_{1.89}Zn_{0.11}]O_4$	8.44085 (10)	0.11	21	385	9.3×10^2	2.0×10^5	1.3

[a] D, particle size (major dimension); a, unit cell parameter; x, inversion parameter; T_B, blocking temperature; $H_{C,5}$, coercive field at 5 K; μ_{SP}, effective superparamagnetic moment; K anisotropy constant; and $M_{S,5}$, saturation moment at 5 K.

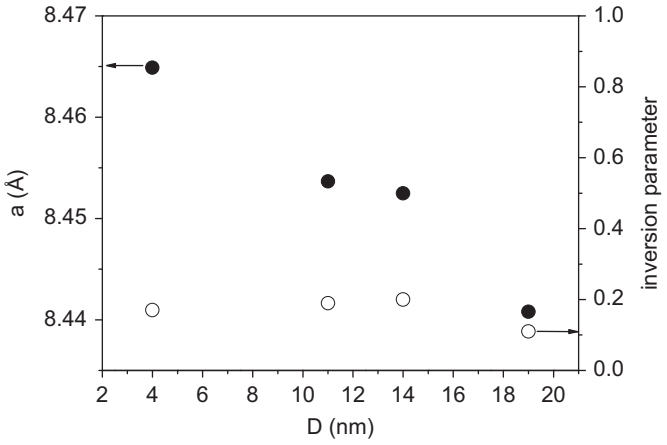

Fig. 4. Unit cell and inversion degree parameters as function of the particle size.

only one that presents the characteristic unit cell parameter $a=8.44$ Å of the bulk normal spinel. The relative large particle size together with the almost unaltered cation distribution respect to the normal spinel $ZnFe_2O_4$ allows this sample to preserve such characteristic length. On the other hand, Z11 and Z14MW samples show a higher unit cell parameter $a=8.45367(10)$ and $a=8.45256(10)$ Å, respectively, corresponding to a more random cation distribution and a lower particle size. Furthermore, the slightly higher value of a corresponding to Z14MW sample could be related with its higher disordered cation distribution. In the case of Z4 sample not only the random cation distribution but also the low particle size contributes to the increasing of the unit cell parameter value. Both effects [24,30] fully justify the obtained $a=8.46498(15)$ Å value.

The magnetic susceptibility versus temperature for both ZFC and FC processes is depicted in Fig. 5a for all the samples. The T_B value for each sample has been estimated from the ZFC maximum (Table 2) and the derivative of $(\chi_{FC}-\chi_{ZFC})$ plot that reflects the particle size distributions is depicted in the inset of Fig. 5a for each sample. The high values of susceptibility reveal that, in all the cases, the ferrite nanoparticles behave as superparamagnetic above the T_B. At low temperature the magnetic susceptibility increases as the particle size increases from 4 to 14 nm (Z4 to Z14MW sample) because in single-domain nanoparticles, the magnetization and therefore the magnetic susceptibility are affected by the coupled moment carriers amount that increases when the particle size increases [31]. This can be understood taking into account that, as the spins surface is canted, the proportion of coupled moment carriers decreases when the particle size becomes smaller due to the increment of the surface/volume ratio [32,33]. In the case of Z19 sample, its ZFC and FC susceptibility curves present very low values because the only visible effect is the inversion degree due to its low surface/volume ratio. On the contrary, the high values of susceptibility that Z14 MW sample presents can be related with its higher inversion degree, thus increasing the proportion of coupled moment carriers in the particles.

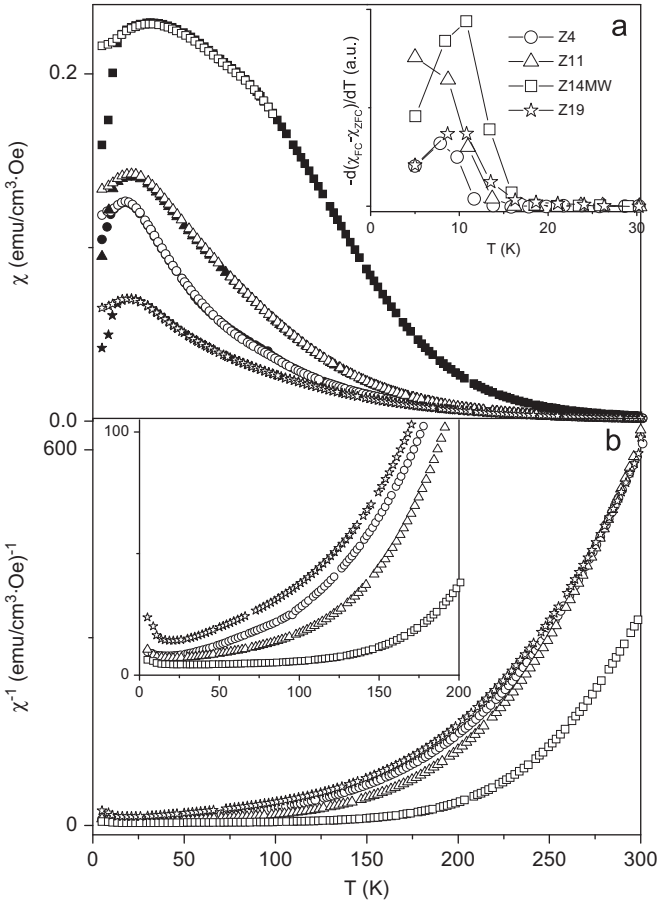

Fig. 5. (a) ZFC and FC magnetic susceptibility for the different $ZnFe_2O_4$ samples. Inset shows the $-d(\chi_{FC}-\chi_{ZFC})/dT$ plots obtained from the magnetic susceptibility measurements. (b) Inverse of the magnetic susceptibility versus temperature for all the obtained samples. Inset shows the 5–200 K temperature range of the mentioned plots.

In absence of an external magnetic field, the anisotropy energy for an uniaxial and single-domain particle can be described by the Stoner–Wolfhart formula [34]:

$$E_a = KV\sin^2\theta$$

where K is the anisotropy constant, V is the particle volume and θ is the angle between the easy axis of the particle and the applied magnetic field), where KV is the anisotropy barrier (U) that if it is overcome by the thermal energy, the particle magnetic moment is able to rotate (superparamagnetic regime). The well known Néel–Brown [35] expression establishes the relation between U and T_B:

$$\tau = \tau_0 \exp\left(\frac{U}{K_B T}\right)$$

where τ_m is the measuring time, τ_0 is the characteristic time and k_B is the Boltzman constant, which implies that the particle size distribution determines the T_B distribution. Inset of Fig. 5a shows the $-d(\chi_{FC}-\chi_{ZFC})/dT$ curve that reflects the particle size distribution [36,37]. As it can be seen from the plots, all the samples are monodisperse. On the other hand, while Z4, Z11 and Z19 samples present similar T_B values (from 18 to 22 K) (see Table 2), evidencing very similar anisotropy barriers at 500 Oe, Z14MW sample presents a broad ZFC maximum and a higher T_B value (35 K) (see Fig. 5a and Table 2). This can be attributed to two main effects: the presence of dipolar particle interactions and a heterogeneous particle size distribution; but taking into account that the $-d(\chi_{FC}-\chi_{ZFC})/dT$ plot reveals a monodisperse sample (inset Fig. 5a), only the first effect can justify the T_B value and the width of the ZFC maximum [38,39].

In Fig. 5b the inverse of the magnetic susceptibility versus temperature is depicted for all the samples in the 5–300 K range. It can be clearly distinguished two different slopes corresponding to the two Curie–Weiss behaviors that describe the superparamagnetic and paramagnetic regimes, respectively. As it can be observed, Z14MW sample presents a larger temperature range, from 35 K (T_B) to 175 K approximately, in which the sample illustrates superparamagnetic behavior.

It is well known the Langevin [4] expression that describes the temperature and magnetic field dependence of the magnetization:

$$M(H,T)=\frac{N\mu^2 H}{3\kappa_B T}$$

Therefore, the susceptibility for a superparamagnetic particle is described by the well-known Curie law:

$$\chi_{SP}=\frac{M}{H}=\frac{N\mu^2}{3\kappa_B T}=\frac{Ms\mu}{3\kappa_B T}$$

where $\mu=MsV$, and $N=1/V$ is the density of particles per unit volume.

The magnitude of μ characteristic of each behavior can be calculated from the slope of the $1/\chi$ versus T plot. In this sense, it has been calculated the effective magnetic moment corresponding to the superparamagnetic regime (μ_{SP}) for each sample (Table 2). It can be seen in the following order: $\mu_{SP\_Z14MW} \gg \mu_{SP\_Z11} > \mu_{SP\_Z19} > \mu_{SP\_Z4}$. The effective μ_{SP} value depends on the amount of coupled moments carriers, which is proportional to the particle size and the inversion degree parameter. Thus, Z19 sample presents very low μ_{SP} taking into account its relatively large particle size, because it presents a low value of inversion degree ($x=0.11$). The low fraction of Fe^{3+} that occupie A-sites in Z19 sample provokes a weak ferrimagnetic correlations inside the particle causing the low value of μ_{SP}. Although Z4 sample presents a lower μ_{SP} value than that corresponding to Z19 sample, it is slightly higher than expected taking into account its low particle size. But this fact is understood considering its higher inversion degree. The Z11 sample presents higher μ_{SP} than Z4 and Z19 samples because it exhibits higher inversion degree and a relative large particle size. In the case of the Z14MW sample, both parameters are large and therefore the sample presents the highest magnitude of μ_{SP}. This large value of μ_{SP} would justify the dipolar particle interactions that previously have been considered, the cause of the higher T_B value and a broader ZFC curve.

Magnetization versus applied field (M versus H) measured at 5 and 250 K is plotted for all the samples in Fig. 6a and b, respectively. All the samples present a hysteresis loop at 5 K typical of a ferrimagnetic material. The coercive field (H_C), saturation moment (M_S) and anisotropy constant (K) corresponding to the different samples are collected in Table 2. The M_S and K values were obtained from M versus H experimental data fitting

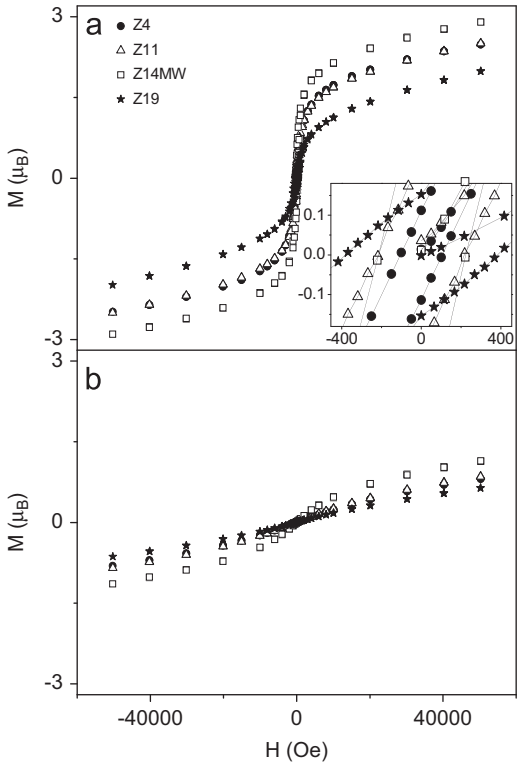

Fig. 6. (a) Magnetization versus applied field hysteresis loops measured at 5 K for all the $ZnFe_2O_4$ samples. Inset shows an augment of the plots. (b) Magnetization versus applied field hysteresis loops measured at 250 K for all the $ZnFe_2O_4$ samples.

in the 1–50 KOe range to the approach to saturation law:

$$M(T)=M_S\left(1-\frac{a}{\sqrt{H}}-\frac{b}{H^2}\right)+cH$$

$$b=\frac{8}{105}\frac{K^2}{M_S^2}$$

where a is a constant, and c is the magnetic susceptibility in the field range indicated.

As the M_S value reflects the inversion degree of each sample, it could be said that the obtained data is in agreement with the calculated inversion degree. Thus, while Z19 sample presents the lowest M_S value due to its lowest inversion degree, Z14MW sample that presents the highest x parameter also has the highest M_S value. Finally, Z4 and Z11 samples present similar M_S values because their inversion degree parameters are also very similar.

It can be seen from Table 2, a general trend of diminishing the anisotropy constant value as the particle size increases (although Z14MW presents a slightly lower value). A similar trend has been previously found in solvothermally obtained nanoparticles whose anisotropy constants were estimated from Mössbauer spectroscopy [40]. This fact is related with the increase in surface/volume ratio as the particle size decreases. In this sense, as the particle size gets reduced, the surface anisotropy gains importance and the effective anisotropy is larger.

The critical particle size (17 nm) for $ZnFe_2O_4$ nanoparticles was estimated from the H_C versus particle size plot at 5 K in a previous work [25]. Below such value, it was observed an augment of the H_C value with the particle size corresponding to the single-domain regime [31]. This trend can be observed as well from Z4 to Z14MW samples, and Z19 sample would belong to the multi-domain regime. Taking into account that the corresponding H_C value to the critical particle size (17 nm) is 450 Oe, it seems to

be that the H_C value that corresponds to Z14MW sample (215 Oe) does not follow this trend as it is lower. It has been pointed out in other works that the surface anisotropy seems to control the H_C parameter [41]. In this case, the particle interaction that this sample seems to present would slightly decrease the surface anisotropy causing a lower value of the H_C parameter [42,43] and the effective anisotropy constant (see Table 2).

The M versus H plot at 250 K (Fig. 6b) for all the samples reveals an almost paramagnetic behavior with low magnetization regardless of the applied field. In the case of the Z14MW sample, the M versus H curve shows higher M_S value. This is in agreement with its inverse susceptibility curve that shows a lower loss of the effective magnetic moment at that temperature, compared with the rest of the samples, as it can be seen in Fig. 5b.

4. Conclusions

Nanosized $ZnFe_2O_4$ particles with sizes of 4, 11 and 19 nm have been prepared by the solvothermal method. Another sample of 14 nm particle size has been synthesized by microwave assisted solvothermal method. Neutron powder diffraction measurements at room temperature reveal an increasing inversion degree from Z19 to Z11 sample due to the reduction of the particle size. The Z14MW sample presents a slightly higher x parameter corroborating the effect of the synthesis conditions in the inversion degree. On the other hand, Z4 sample exhibits a lower inversion degree due to its small particle size. It has been found that the unit cell parameter increases with the decreasing of particle size and increment of the x value. On the other hand, the sample obtained by microwave-assistance presents a slightly higher value of a, which agrees with its slightly high value of x.

All the samples behave as superparamagnetic and they seem to be monodisperse as their $-d(\chi_{FC}-\chi_{ZFC})/dT$ plots indicate. This leads to believe that the broad ZFC maximum in the case of the sample obtained by microwave assistance is a consequence of dipolar particle interactions probably related with the higher inversion degree and μ_{SP}.

The M versus H hysteresis loops at 5 K indicate that all the samples behave as ferrimagnetic at that temperature. It has been calculated the M_S and K for all the samples after fitting the experimental data to the approach of saturation law. It has been found a decreasing K value with the augment of the particle size, and also that the M_S values are in agreement with the calculated inversion degree for each sample. The sample obtained by microwave assistance presents a slightly low value of H_C and K, which can be justified under the consideration of particle interactions.

Acknowledgments

The authors are grateful to the Ministerio de Ciencia e Innovación for the financial support under project MAT 2010-19460 and Universidad Complutense de Madrid for a predoctoral grant. The authors also thank "Centro de Microscopía Electrónica" and "CAI de difracción de Rayos X" at UCM for the technical assistance.

References

[1] C. Vázquez-Vázquez, M.A. López-Quintela, M.C. Buján-Núñez, J. Rivas, J. Nanopart. Res. (2010). doi:10.1007/s11051-010-9920-7.
[2] X. Batlle, A. Labarta, J. Phys. D: Appl. Phys. 35 (2002) R15–R42.
[3] P. Tartaj, Eur. J. Inorg. Chem. (2009) 333–343.
[4] M. Knobel, W.C. Nunes, L.M. Socolovsky, E. De Biasi, J.M. Vargas, J.C. Denardin, J. Nanosci. Nanotechnol. 8 (6) (2008) 2836–2857.
[5] O. Petracic, Superlattices Microstruct. 47 (5) (2010) 569–578.
[6] Guilherme V.M. Jacintho, Alexandre G. Brolo, P. Corio, Paulo A.Z. Suarez, Joel C. Rubim, J. Phys. Chem. C 113 (18) (2009) 7684–7691.
[7] V. Musat, O. Potecasu, R. Belea, P. Alexandru, Mater. Sci. Eng: B 167 (2) (2010) 85–90.
[8] F. Einar Kruis, H. Fissan, A. Peled, J. Aerosol Sci. 29 (5–6) (1998) 511–535.
[9] M. Arruebo, R. Fernandez-Pacheco, M.R. Ibarra, J. Santamaría, Nano Today 2 (3) (2007) 22–32.
[10] S. Laurent, D. Forge, M. Port, A. Roch, C. Robic, L. Vander Elst, R.N. Muller, Chem. Rev. 108 (2008) 2064–2110.
[11] H.H. Hamdeh, J.C. Ho, S.A. Oliver, R.J. Willey, J. Kramer, Y.Y. Chen, S.H. Lin, Y.D. Yao, M. Daturi, G. Busca, IEEE Trans. Magnet. 31 (6) (1995) 3808–3810.
[12] W. Schiessl, W. Potzel, H. Karzel, M. Steiner, G.M. Kalvius, A. Martin, M.K. Krause, I. Halevy, J. Gal, W. Schäfer, G. Will, M. Hillberg, R. Wäppling, Phys. Rev. B 53 (1996) 9143–9152.
[13] J.M. Hastings, L.M. Corliss, Phys. Rev. 102 (6) (1956) 1460–1463.
[14] V. Nachbaur, G. Tauvel, T. Verdier, M. Jean, J. Juraszek, D. Houvet, J. Alloys Compd. 473 (2009) 303–307.
[15] C.N. Chinnasamy, A. Narayanasamy, N. Ponpandian, K. Chattopadhyay, Mater. Sci. Eng. A 304–306 (2001) 983–987.
[16] S.A. Oliver, V.G. Harris, H.H. Hamdeh, J.C. Ho, Appl. Phys. Lett. 76 (19) (2000) 2761–2763.
[17] H.H. Hamdeh, J.C. Ho, Phys. Rev. B 60 (5) (1999) 3400–3405.
[18] V. Blanco-Gutierrez, F. Jimenez-Villacorta, P. Bonville, Maria J. Torralvo-Fernandez, R. Saez-Puche, J. Phys. Chem. C 115 (5) (2011) 1627–1634.
[19] F.S. Li, L. Wang, J.B. Wang, Q.G. Zhou, X.Z. Zhou, H.P. Kunkel, G. Williams, J. Magn. Magn. Mater. 268 (2004) 332–339.
[20] S.J. Stewart, S.J.A. Figueroa, M.B. Sturla, R.B. Scorzelli, F. García, F.G. Requejo, Physica B 389 (2007) 155–158.
[21] J.H. Shim, S. Lee, J.H. Park, S.-J. Han, Y.H. Jeong, Y.W. Cho, Phys. Rev. B 73 (2006) 064404-4.
[22] Z.J. Zhang, Z.L. Wang, B.C. Chakoumakos, J.S. Yin, J. Am. Chem. Soc. 120 (1998) 1800–1804.
[23] M. Hofmann, S.J. Campbell, H. Ehrhardt, R. Feyerherm, J. Mater. Sci. 39 (2004) 5057–5065.
[24] F. Braestrup, B.C. Hauback, K.K. Hansen, J. Solid State Chem. 181 (2008) 2364–2369.
[25] V. Blanco-Gutierrez, Maria J. Torralvo-Fernandez, R. Saez-Puche, J. Phys. Chem. C 114 (2010) 1789–1795.
[26] M. Järvinen, J. Appl. Crystallogr. 26 (1993) 525–531.
[27] A.L. Patterson, Phys. Rev. 56 (1939) 978–982.
[28] S. Ammar, N. Jouini, F. Fievet, O. Stephan, C. Marhic, M. Richard, F. Villain, Ch. Cartier dit Moulin, S. Brice, Ph. Sainctavit, J. Non-Cryst. Solids 345&346 (2004) 658–662.
[29] P. Druska, U. Steinike, V. Sepelak, J. Solid State Chem. 146 (1999) 13–21.
[30] M. Fukuhara, Phys. Lett. A (2003) 427–430.
[31] A.H. Lu, E.L. Salabas, F. Schüth, Angew. Chem. Int. Ed. 46 (2007) 1222–1244.
[32] G.C. Hadjipanayis, J. Magn. Magn. Mater. 200 (1999) 373–391.
[33] M. George, A.M. John, S.S. Nair, P.A. Joy, M.R. Anantharaman, J. Magn. Magn. Mater. 302 (2006) 190–195.
[34] E.S. Stoner, E.P. Wohlfarth, Philos. Trans. R. Soc. Lond., Ser. A 240 (826) (1948) 599–642.
[35] W.F. Brown, Phys. Rev. 130 (1963) 1677–1686.
[36] J.C. Denardin, A.L. Brandl, M. Knobel, P. Panissod, A.B. Pakhomov, H. Liu, X.X. Zhang, Phys. Rev. B 65 (2002) 064422–064428.
[37] J.M. Vargas, E. Lima Jr., R.D. Zysler, J.G.S. Duque, E. De Biasi, M. Knobel, Eur. Phys. J. B 64 (2008) 211–218.
[38] E.E. Carpenter, J.W. Long, D.R. Rolison, M.S. Logan, K. Pettigrew, R.M. Stroud, L.T. Kuhn, B.R. Hansen, S. Mørup, J. Appl. Phys. 99 (2006) 08N711–08N713.
[39] Y. Sahoo, Y. He, M.T. Swihart, S. Wang, H. Luo, E.P. Furlani, P.N. Prasad, J. Appl. Phys. 98 (2005) 054306–054309.
[40] V. Blanco-Gutierrez, M.J. Torralvo, R. Saez-Puche, P. Bonville, J. Phys. Proc. ICM 2009 (200) (2010) 072013–072014.
[41] C.R. Vestal, Z.J. Zhang, J. Am. Chem. Soc. 125 (2003) 9828–9833.
[42] V. Blanco-Gutierrez, E. Urones-Garrote, M.J. Torralvo-Fernandez, R. Saez-Puche, Chem. Mater. 22 (22) (2010) 6130–6138.
[43] Y. Zhu, W. Zhao, H. Chen, J. Shi, J. Phys. Chem. C 111 (2007) 5281–5285.